

©2023. Elsevier. This manuscript version is made available under the CC-BY-NC-ND 4.0 license  
<http://creativecommons.org/licenses/by-nc-nd/4.0/>

**This item is the archived peer-reviewed author-version of:  
Catalytic performance of rGO-Zeolite modified anode in clay biophotovoltaics system for  
effective urine treatment**

**Reference:**

Gunaseelan, K., Jadhav, D.A., Pant, D. and Gajalakshmi, S., 2023. Catalytic performance of rGO-Zeolite modified anode in clay biophotovoltaics system for effective urine treatment. **International Journal of Hydrogen Energy**, 48(3), pp.1160-1174.

ISSN 1879-3487 (2023), Copyright © 2023 Elsevier. All rights reserved

Full text (Publisher's DOI): <https://doi.org/10.1016/j.ijhydene.2022.09.216>

Received 11 March 2022; Received in revised form 25 August 2022; Accepted 23 September 2022

**Catalytic performance of rGO-Zeolite modified anode in clay Biophotovoltaics system  
for effective urine treatment**

K. Gunaseelan<sup>1</sup>, Dipak A. Jadhav<sup>2,3</sup>, Deepak Pant<sup>4</sup>, S. Gajalakshmi<sup>1\*</sup>

<sup>1</sup>Sustainable Fuel Cells Technology Lab, Centre for Pollution Control & Environmental  
Engineering, Pondicherry University, Puducherry-605 014, India

<sup>2</sup>Department of Agricultural Engineering, Maharashtra Institute of Technology, Aurangabad  
– 431010, India

<sup>3</sup>Department of Environmental Engineering, College of Ocean Science and Engineering,  
Korea Maritime and Ocean University, 727 Taejong-ro, Yeongdo-gu, Busan, 49112,  
Republic of Korea

<sup>4</sup>Separation and Conversion Technology, Flemish Institute for Technological Research (VITO),  
Boeretang 200, 2400 Mol, Belgium

\*Corresponding Author: Email: [dr.s.gajalakshmi@gmail.com](mailto:dr.s.gajalakshmi@gmail.com);  
[gajalakshmi.cpe@pondiuni.edu.in](mailto:gajalakshmi.cpe@pondiuni.edu.in)

## **Abstract**

Low power output due to poor anode kinetics is minimized by modifying the anode with rGO-Zeolite to improve the electrochemical redox reactions in biophotovoltaics (BPV). Higher power production and N/P- recovery is successfully achieved in horizontal Torch separator-based urine fed BPV modified with rGO-Zeolite anodes than bare graphite anode. Among the two variants of anodes, modified anode results in power of 146.88 mW/m<sup>2</sup>, redox current of 18.9 mA, Phosphorous ( $88 \pm 0.3\%$ ), NH<sub>4</sub>-N ( $49 \pm 0.5\%$ ), and Coulombic efficiency of  $15.16 \pm 0.3\%$ . Improvement in power output is due to the higher electroactive surface area provided by rGO-Zeolite anode for electron transfer. Recovery of clear catholyte (8 ml/day) during human-urine treatment and energy recovery for operating the hygro-clock are the main key features of low-cost BPV. Thus, BPV with modified anodes serves as a sustainable technology for recovering energy and resources from human urine and makes it suitable to use for onsite urine treatment and sanitation applications.

**Keywords:** Anode modification; Biophotovoltaics; Clay torch separators; Direct powering, Urine treatment; Struvite recovery

## 1. Introduction

A bioelectrochemical system (BES) can convert chemical energy from existing organic contaminants in wastewater into electrical energy under anaerobic conditions through microbial metabolism [1–3]. The most recent techniques for harnessing solar energy to generate electricity are biophotovoltaics (BPVs) or photo-MFCs [4]. BPVs may be carried out employing oxygenic or anoxygenic photosynthetic bacteria, depending on their photosynthetic mechanism [5]. Despite the fact that there is a growing interest in utilizing photoautotrophs to treat wastewater with a low carbon footprint, the technology is still in its early stages and is unable to reach the maximum theoretical values necessary for real-world applications [6,7].

Urine is in general flushed down the toilet and treated at wastewater treatment plants (WWTPs) before being released into natural water bodies [8–10]. Phosphorus (P) and nitrogen (N) are two major constituents that must be removed from wastewater because their accumulation can cause freshwater eutrophication in water bodies, which can cause severe socioeconomic and ecological damage [11–13]. As a result, most current WWTPs use energy-intensive treatment methods to remove both phosphorus and nitrogen, which are also extremely expensive to construct and maintain. Both N and P may be recovered concurrently from the mainline of urine wastewater using the vertically positioned clay separator based air-cathode / single-chambered Microbial fuel cells (MFC) by precipitating them in the form of struvite (Magnesium ammonium phosphate- $\text{MgNH}_4\text{PO}_4 \cdot 6\text{H}_2\text{O}$ ) which is commonly identified as the slow-releasing fertilizer [14–16]. Using waste to recover useful resources is a novel way to clean production with substantial environmental and economic benefits [17–19].

Being one of the primary components for BPV fabrication, the anode, which promotes the growth of electroactive bacteria and the development of microbial biofilm, is essential to

the reactor's performance. Biofilm development over the anodes with photoautotrophs and heterogeneous microorganisms is thought to be beneficial in attaining increased power production in BES [5]. Furthermore, photoautotrophs are thought to be utilized as organic feedstock for heterotroph survival, as well as the free electrons released through the oxidation process of those organic molecules. Several edifying research is being carried out to develop cost-effective modified anodes for BES applications.

Graphene-modified electrodes show potential for BES development by overcoming the productivity loss caused during the conversion of organic pollutants into electrical energy [20–22]. Quite a few studies have been published on the modification of anodic materials such as NiWO<sub>4</sub>-GO [23], polyaniline-rGO [24], and biosynthesized graphene oxide (GO) [25] with the higher power density of 1458, 306, and 1158 mW/m<sup>2</sup> respectively than the MFCs with the bare anodes and nano-hybrid graphene and titanium dioxide as a cathode in MFCs [26]. Due to reduced graphene oxide (rGO) with high electrical conductivity (106 Sm<sup>-1</sup>), traditional carbon-based electrodes are frequently improved with graphene scaffold to minimize interfacial charge-transfer resistance and increase extracellular electron transfer (EET) performance [27]. However, poor anode kinetics in bare anode leads to the search for effective low-cost anode modification for improving the electrochemical redox reactions.

The modification of the anodes with the combination of zeolite and graphite/graphene gained the attention of the researchers due to the super-hydrophilicity characteristics of zeolite which accelerated the thick biofilm formation [28]. The cells clump together to form an interconnected biofilm network that binds multiple layers of graphene nanosheets via macropores [29]. Zeolite-modified electrodes (ZMEs) can promote ion exchange [30] without undergoing severe structural change and are not influenced by shrink-swell modifications due to their three-dimensional solid network [31]. The studies on Faujasite zeolite- graphite electrodes [28], and zeolite-GO modified graphite felt anode [32] testified with a peak power

density of 152% and 360% respectively than the MFCs without modified anodes. Like anode, cation exchange membrane accounts for around 60% of the material cost of BES in scale-up applications, thus clay/ceramic separator is considered to be suitable for a wide range of applications due to cost savings and enhanced power production efficiency [33,34]. Because of its high thermal resilience, physical integrity, and chemical resistance, ceramic membranes are suitable for harsh cleaning conditions such as acid or alkaline washing, as well as physical cleaning processes [35].

Recent research focuses on MFC integration with membrane separation process to treat effluent [36], based on the process such as electro-osmosis and catholyte production, this gives hope of using the ceramic-based MFC for filtering the anolyte through electro-osmotic drag. So, that clear catholyte can be produced along with electricity generation instead of consumption [37,38]. The electro-osmotic drag is an important phenomenon of ceramic separator-based BES, in particular, is the movement of water molecules along with protons passing which is self-driven from the anode to the cathode via a separator as a clear catholyte. This filtration and water recovery from neat human urine can also be correlated directly to the current produced by the fuel cells [37,38].

In the present study, the novel low-cost horizontally positioned torch type clay separator for human urine fed air-cathode BPV with rGO and Zeolite modified Graphite felt anode was fabricated and evaluated for their suitability in a simple, tetra-generative system (i) to enhance electricity generation ability for scale-up the system for real-world applications, (ii) to treat neat human urine effectively, (iii) struvite recovery (slow-release fertilizer), and (iv) collecting clear catholyte. The novelty of this urine fed BPV is in the operational simplicity, and particularly self-sustainable in recovering the collected clear catholyte at ease without using any additional pump /suction gadgets [39,40] due to the horizontally positioned torch type clay separator, unlike the reported works on MFC with vertical ceramic separators

[41,42]. Further, this study investigates the long-term reliability and direct powering of hygro-clock to ensure the suitability of the novel horizontally positioned torch-type air-cathode urine BPVs for real-time onsite sanitation applications and scale-up studies.

## **2. Materials and methods**

### **2.1 Fabrication of torch type clay separator**

Terracotta clay was used to make the torch-shaped separator with the help of the professionally skilled pot maker by the traditional hand throwing technique over the rotating wheels. The hand-thrown torch-shaped separators were dried under the shade for one week at room temperature. After drying, these torch-shaped separators were kilned at 650°C in the muffle furnace for 1 hour. The uniformly kilned separators without any cracks and structural deformations were utilized for the fabrication of torch-type urine-fed BPV variants.

### **2.2 Substrate and biocatalyst**

Freshly collected neat human urine was utilized as the anolyte for the operation of torch-type urine-fed BPV variants. The feed urine was collected from the urinals of the University Department. The BPVs were inoculated with SUPER-MIX inoculum obtained from a long-time running BPVs from our laboratory [43].

### **2.3 BPV setup and operation**

Single chambered air cathode BPV reactors were fabricated using cylindrical transparent low-density polyethylene (LDPE) containers (Fig.1). The synthesis of GO and rGO were carried out by Paul et al., 2018 [32], and Gautam et al., 2016 [32], respectively. The torch-shaped separator was fixed horizontally as the physical separator along with the 3-Dimensional anode materials of interest, namely the rGO- zeolite modified anode (rGOZA) and unmodified graphite felt anode (UMA) internally and the commonly adopted air cathode with the gas diffusion layer (GDL) on the external face [44,45]. The clay torch type

separators-based urine BPV with rGOZA and UMA have coined the names rGOZA BPVs and UMA BPVs, respectively. Each cylindrical urine BPV is of a working volume of 600 mL and provided with two ports, one for anodic wire and the other as a common port for the sampling of the urine and reference electrode. In common, all the BPVs were equipped with the dimension of 25 cm<sup>2</sup> anodes and 50 cm<sup>2</sup> cathodes, respectively offering more electrochemical active surface area for electrochemical redox reactions. Initially, both the variants of BPVs were operated under closed-circuit conditions by introducing the external load of 1000  $\Omega$  during the start-up phase and which was then gradually connected to the lower resistance of 100  $\Omega$ , reported with steady and stable performance [46]. To maintain the anaerobic state, the anodic chambers of all the BPVs were sparged with 99.9% N<sub>2</sub> gas during the feeding of the substrate and sampling [4]. Higher COD reduction and consistent voltage outputs at room temperature (29.2°C) indicate that the BPVs have stabilized in their performance. All of the BPVs were exposed for 12 hours to red-blue light with wavelengths of 715-1050 nm, and 450-550 nm, followed by 12 hours of darkness [47].



**Fig. 1** Hygro-clocks direct powering ability of the rGOZA and UMA BPVs

## **2.4 Characterization of GO, rGO, and recovered resource**

The samples were analyzed using an Invia Reflex Raman Microscope, Renishaw Metrological Systems UK with a laser excitation of 785 nm for graphitic structures, disordered phases, and defects in synthesized catalysts. An X-ray diffractometer (Shimadzu XRD 7000) with Cu K value of 1.54060 radiations at a speed of 2°/min, diffraction angle of 2θ from 10° to 40° at 40 kV and 30mA was used to investigate the crystalline patterns and crystallinity of the fabricated nanoparticles and recovered struvite crystals. The anolyte supernatant was removed from the anodic chamber, and leftover slurry was collected, and air-dried for 48 h for complete dehydration and solidification. The solidified crystals samples were analyzed for XRD and FTIR analysis [37]. The recovered struvite-like crystal's FTIR spectra were acquired at room temperature using an FTIR Spectrophotometer (Thermo Nicolet Model: 6700, UK). The spectra were obtained between 400 and 4000 cm<sup>-1</sup>, and the calibration was done with KBr as a blank. X-ray Photoelectron Spectrometry (XPS) from Thermo Scientific K-Alpha-KAN9954133 was used to examine the elemental constituents and their bonding state on, surface, and near-surface layers of synthesized GO, rGO, and recovered resource (struvite) [48]. Morphological characteristics of the synthesized GO and rGO nanoparticles, followed by the modified anode variants were observed by using Scanning Electron Microscope. Small portions of anode variants were cut into small pieces of 3 mm × 3 mm and carbon ion sputtering is done on the pieces in HITACHIE-1010 sputter for a homogeneous coating. The images of the samples were from S3400N Scanning Electron Microscope with 15kV incident electron beam energy of and 50.0μm working distance .

## **2.5 Electrochemical analyses and pollutant removal efficiency**

Using a polarization curve, the electrogenic activities of torch type urine fed BPVs (operated in batch mode) with modified anodes were evaluated as voltage, current, and power

density [4,49]. A digital multi-meter (Sanwa CD772) was utilized to evaluate the open-circuit voltage (OCV) of the Clay BPV variants. During the six months of operation, the BPVs were coupled with the 1000 - 100  $\Omega$  resistors to complete the circuit once they had reached stable OCV levels. The acquired current density (CD) against potential, as well as power density (PD), was used to depict polarisation curves for torch-type urine-fed BPV variants. A decade resistor box (Model: CES 1001, Crown Electronic Systems, India) was utilized to perform the Polarization experiments by modifying external resistance between 10 K $\Omega$  to 10  $\Omega$  [50]. The power density values and volumetric power of the BPVs variations were calculated using the anodic surface area and net volume of the anode compartment.

Cyclic voltammetry (CV) is a straightforward approach for determining the oxidation and reduction process at the BES's electrodes. The extent of biofilm electrocatalytic processes of anode can be determined by the redox current peak response at turnover conditions. Under the highly stabilized condition, the maximal redox peak current of the BPV variants with modified and unmodified anodes was investigated. The complete setup comprise of three electrodes: (i) BPV's anode as the working electrode, (ii) Ag/AgCl as the reference electrode, and (iii) BPV's cathode as a counter electrode. CV was done at a slow scan rate of 10 mV/s between -1 to +1 V potential. SQUIDSTAT PLUS Potentiostat (Admiral Instrument, USA) was used to record the response current peaks caused by varying voltage and also to conduct Electrochemical Impedance Spectroscopy (EIS) between 100 kHz to 1 mHz and a 10 mV of frequency and amplitude of AC signal respectively. The solution /ohmic resistance ( $R_s$ ), polarization/charge transfer resistance ( $R_{CT}$ ), and ultimately the Warburg diffusion resistance ( $W_R$ ) were all calculated using the Nyquist plot and equivalent circuit. Bode plot was utilized to estimate the internal resistance of MFC with more clarity about the distribution of resistance with a change in anodic conditions. The Coulombic efficiency at the anode chamber ( $C.E_{an}$ ) was estimated based on the removal

efficacy of chemical oxygen demand (COD) in the BPVs and the amount of current generated. The COD of the anodic wastewater was analyzed after every batch of operation by the open reflux method as per APHA standard methods [51].

### 3. Result and discussion

#### 3.1 Characterization of GO and rGO

The typical Raman Spectra was taken from various regions of graphene oxide. The formation of graphene oxide was identified through the presence of the two distinctive peaks at  $1350\text{ cm}^{-1}$ , and  $1598\text{ cm}^{-1}$  related to the D and G bands, respectively. The D band is attributed to the in-plane breathing vibrational mode of  $A_{1g}$ , which helps in correlating the structural defects as well as partially disordered structures near the edge of the  $sp^2$  Carbon domains. However, the G band was associated with the  $E_{2g}$  vibrational mode of the  $sp^2$  carbon domain which relates to the extent of the graphitization process. Further, the D band and the G band intensity ratio ( $I_D/I_G$ ) evaluate the density of the structural defects in the obtained graphene [45]. For GO and rGO, the  $I_D/I_G$  values were 1.10 and 1.30, respectively. The appearance of disordered carbon or defects during the chemical reduction produced a rise in  $I_D/I_G$  value of rGO compared to GO [45]. The existence of equivalent D and G bands can be observed in rGO. Thus, the formation of GO and rGO were confirmed through Raman spectroscopy (Fig. 2.a).

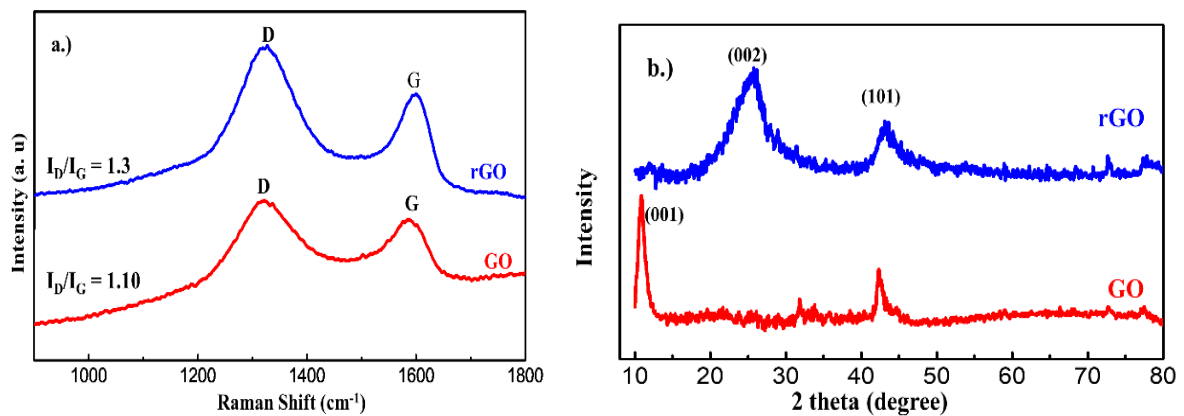
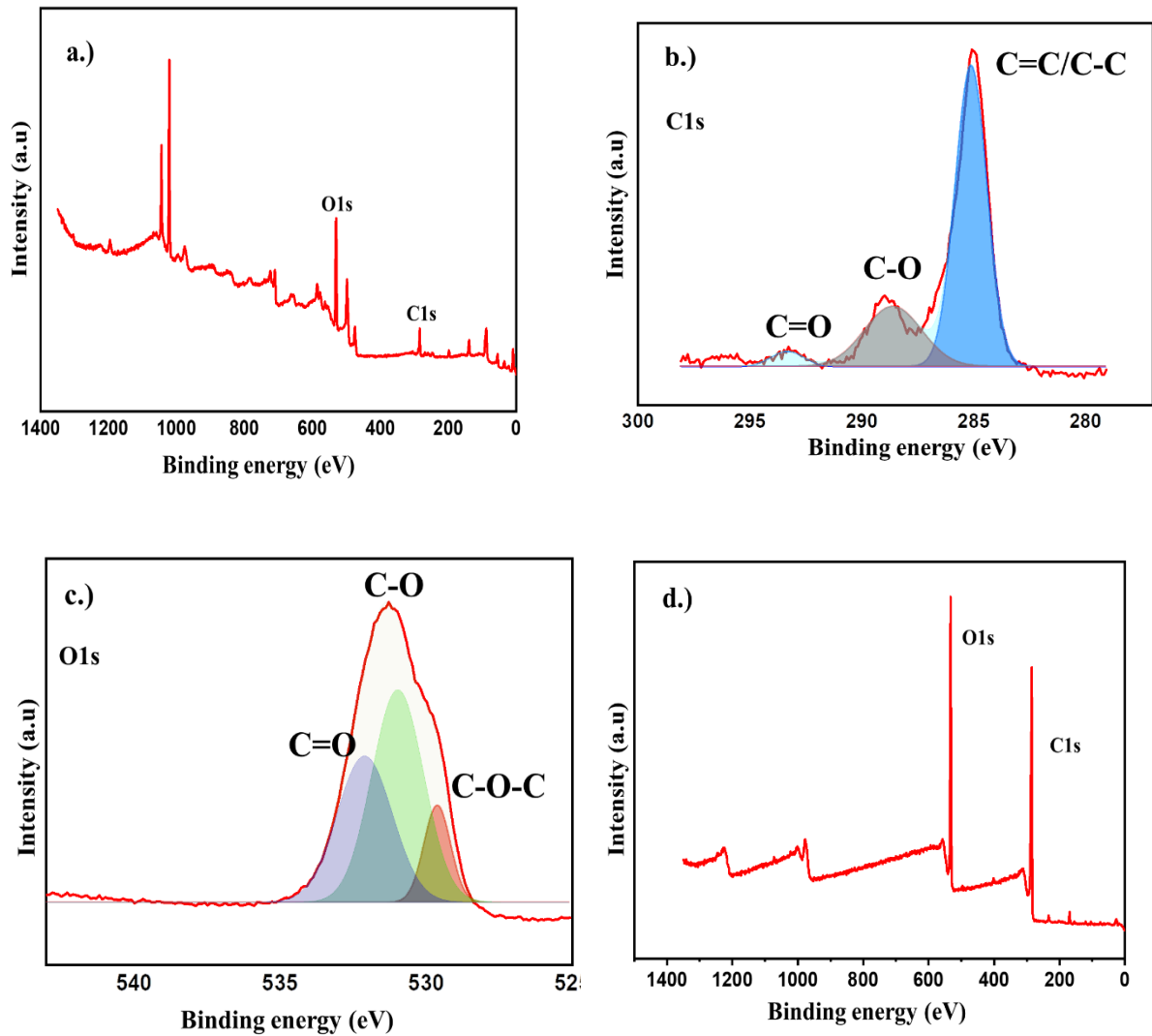


**Fig. 2(a.)** Raman spectra; (b.) XRD spectra of synthesized GO and rGO

The formation of graphene oxide through the modified Hummers method was confirmed by the XRD technique due to the presence of the intense peak at  $10.29^\circ$  which was assigned to the (002) lattice plane. The comparison of the X-ray diffraction of GO and reduced GO or rGO suggests that the reduction of GO to graphene leads to structural change [45]. The synthesis of GO was noticed with a higher interlayer spacing of 0.85 nm as a result of the availability of intercalated functional oxides when compared to graphite with 0.34 nm which confirmed the graphene oxide formation. During the formation of rGO, GO lost most of its intercalated functional oxide groups once it got reduced to form rGO [45]. Using Bragg's law and a wavelength of Cu K of  $1.541 \text{ \AA}$ , the interlayer spacing was calculated from the (002) peak. The sharp diffraction peak at  $2\theta = 10.29^\circ$  disappeared after thermal treatment of GO suggests that the numerous layers were efficiently exfoliated during the thermal reduction of GO [45]. Due to this, the corresponding peak to the 002-lattice plane shifted to a higher angle of  $26.42^\circ$  with a lower interlayer spacing value of 0.33 nm (Fig.2. b). Crystal impurity peaks were not noted, which directed the formation of the high purity of GO and rGO products.

XPS is an efficient technique for determining the surface elemental composition and binding energy of each element. By analyzing the kinetic energy of photoelectrons produced from the valence shell. Because the incoming X-ray penetrates the surface layer upto 10 nm, XPS may examine the surface ligand structure irrespective of particle size [48].GO and rGO sheets XPS spectra were obtained (Fig. 3.a; d). Due to the elimination of oxygen-containing functional groups, there was increase in C/O ratio dramatically after reduction [52]. The degree of oxidation is indicated by the C1s XPS high-resolution spectra of GO (Fig. 3. b). The same functional groups were visible in the C1s XPS spectra of rGO (Fig. 3.e), but with lower intensities and changed peak positions in the oxygen-containing groups. According to

the XPS study, most oxygen-containing functional groups are eliminated, resulting in an increase in  $sp^2$  networks on the rGO basal plane [52]. When compared to GO XPS high-resolution spectra, the peak associated with C 1s becomes more prominent, while the peak associated with O 1s becomes much weaker (Fig. 3. f), indicating that GO has deoxygenated and thereby reduced to rGO during the hydrothermal process [45].



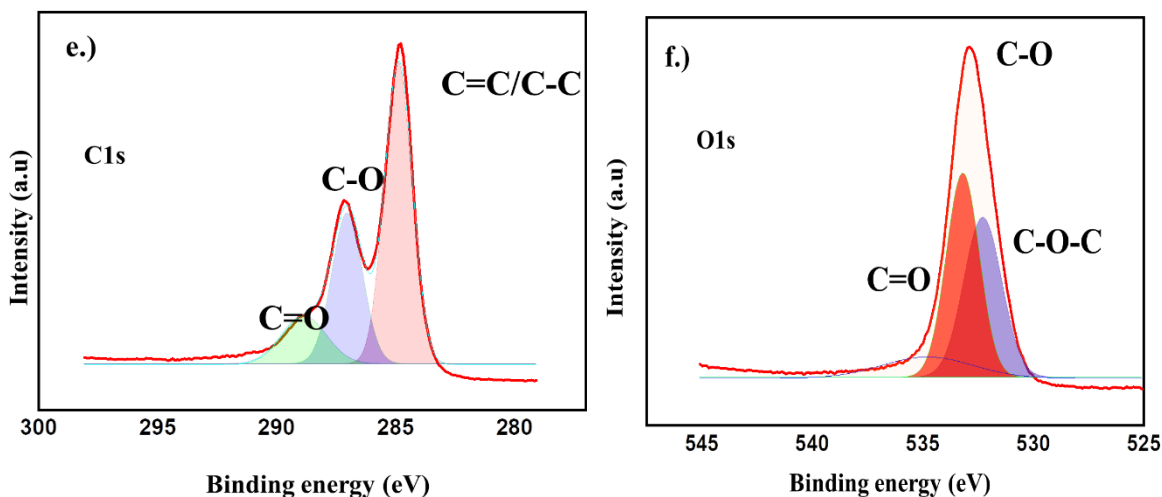


**Fig. 3** XPS survey spectra of (a) GO; (d) rGO, and high-resolution spectra of (b) C1s-GO, (c) O1s-GO, (e) C1s-rGO, and (f) O1s- rGO.

### 3.2 Morphological analysis of modified anode

The confirmation of the rGO and zeolite composites deposition over the graphite felt was done by using SEM micrographs (Fig. 4). It is evident that the zeolite particles were seen entangled along with the rGO sheets. The rGO- zeolite modified graphite felt anode (rGOZA) was known to be incorporated with  $0.57 \text{ mg/cm}^2$  and  $0.28 \text{ mg/cm}^2$  of rGO and zeolite respectively. The rGo-zeolite modified graphite felt was with the zeolite particles over the surface of rGO (Fig.4.d), but in the case of unmodified graphite felt anode (UMA) only the micrometric single standard carbon threads were seen (Fig. 4.c). The tailored method with simultaneous soaking and drying of graphite felts in the rGO-zeolite composite solution resulted in the successfully modified rGO- zeolite graphite felt (Fig. 4.d). The modified graphitic felt with the zeolite led to the super-hydrophilicity of the anode due to its contact angle of  $0^\circ$ . On the other hand, the unmodified graphite felt was super-hydrophobic due to its contact angle of  $180^\circ$  [32]. Furthermore, Zeolite has about  $0.74 \text{ nm}$  pore space, whereas a bacterium has  $0.5 \text{ }\mu\text{m}$ – $3\text{ }\mu\text{m}$  diameter. Due to this, bacterial cells cannot reach the zeolite

surface, nevertheless it aid in improving the movement of polar glucose or acetate molecules, generally used as carbon sources for the microorganisms in MFCs, resulting in improved biofilm growth [53]. Due to this characteristic of the zeolite modified anode aids microbes to acclimate with 2.4 less time, resulting in the rapid formation of biofilm than the bare anode, and also with maximum power density attachment to the anode [24,53]. Following that, enhanced biofilm development was observed with profusely spread spherical shaped bacteria across the surface of the modified anode with rGO and zeolite (Fig. 4.f) than the unmodified anode (Fig. 4.e) due to their exceptional biocompatibility [54].

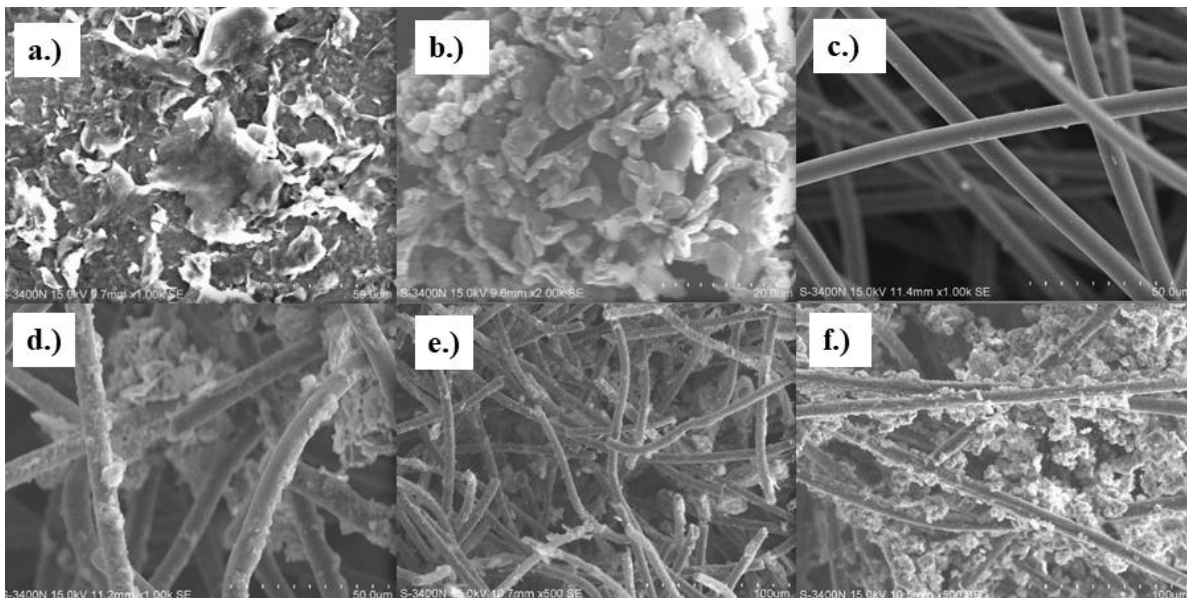


**Fig.4** SEM micrographs of a.) GO; b.) rGO; c.) Unmodified graphite felt; d.) Modified felt with rGO + Zeolite; e.) Unmodified graphite felt with biofilm during 3<sup>rd</sup> batch cycle; f.) rGO + Zeolite modified GF with intense biofilm during 3<sup>rd</sup> batch cycle

### 3.3 Characterization of recovered struvite

The recorded FTIR spectra of recovered struvite samples from both the rGOZA BPV and UMA BPV were compared based on the absorption frequencies, and absorption bonds with the previously reported studies with the pure struvite crystals (Fig. 5.a). The appearance of the broad envelope at  $3157.8\text{ cm}^{-1}$ ;  $3137.4\text{ cm}^{-1}$  represent to O-H and N-H stretching vibrations of struvite samples from rGOZA BPV and UMA BPV respectively. The

absorption band at  $1648\text{ cm}^{-1}$ ;  $1645\text{ cm}^{-1}$ , and  $1404\text{ cm}^{-1}$ ,  $1403.9\text{ cm}^{-1}$  are designated to the N-H bending vibrations of both the BPVs variants struvite samples. The shoulder at  $1147.8\text{ cm}^{-1}$ ;  $1143.7\text{ cm}^{-1}$  is assigned to ammonium ions. The intensified peaks occurring at  $1095.4\text{ cm}^{-1}$ ;  $1096.4\text{ cm}^{-1}$  and  $626.9\text{ cm}^{-1}$ ;  $624.5\text{ cm}^{-1}$  are assigned to  $\nu_3$  and  $\nu_4$  modes of  $\text{PO}_3^{4-}$  ions of both the BPVs variants struvite samples [55].

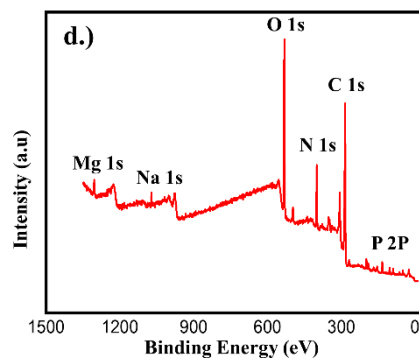
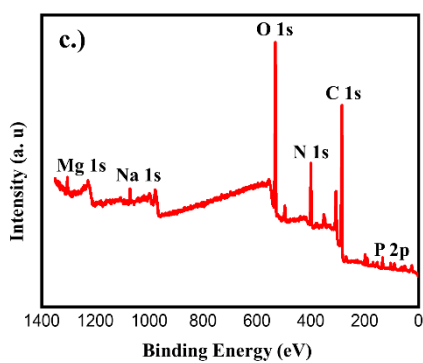
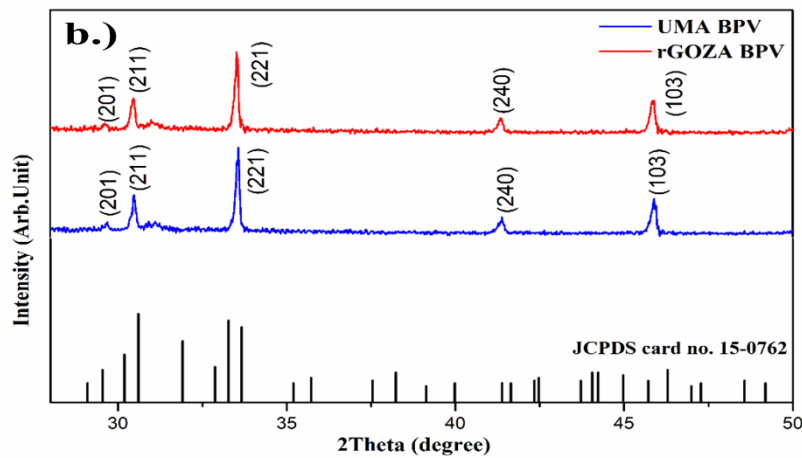
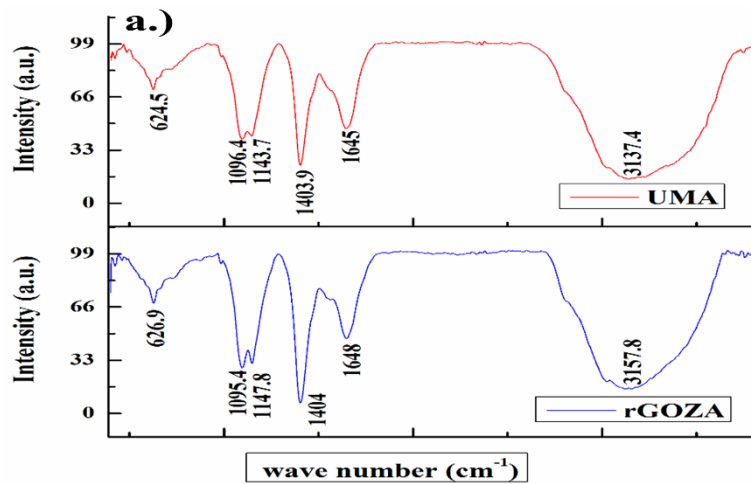


**Fig. 5 a.)** FTIR spectra of recovered struvite from UMA BPV, and rGOZA BPV; b.) XRD spectra of recovered struvite from UMA BPV, and rGOZA BPV; c.) XPS spectra of recovered struvite from UMA BPV; d.) XPS spectra of recovered struvite from rGOZA BPV

The frequency value of all the functional groups confirms the constituents of struvite in the recovered resources of both rGOZA BPV and UMA BPV (Fig. 5.a). The recovered resource as a permeate had a pattern similar to struvite, according to the X-ray diffraction (XRD) study (Fig. S1). The XRD patterns of UMA and rGOZA BPV showed that high-intensity diffraction peaks appeared at 29.5° (201), 30.6° (211), 33.6° (221), 41.3° (240), and 46.2° (103) with variations in peak intensities, which exactly fit with some of the struvite standard peaks (JCPDS card no.15-0762). However, the XRD pattern position and intensity of the peak of XRD obtained from struvite crystals coincided with the reference values of struvite synthesized by a previous study on neat human urine-fed MFC [37]. The purity of the recovered struvite is less due to the presence of other minerals such as epsomite ( $\text{MgSO}_4\text{H}_2\text{O}$ ), montgomeryite ( $\text{Ca}_4\text{Al}_5(\text{PO}_4)_6(\text{OH})_{5.11}\text{H}_2\text{O}$ ,  $\text{Ca}_4\text{MgAl}_4(\text{PO}_4)_6(\text{OH})_{4.12}\text{H}_2\text{O}$ ), and brucite ( $\text{Mg}(\text{OH})_2$ ) [56].

The surface composition of the struvite sample from UMA BPV and rGOZA were further examined by XPS over the energy range of 0–1350 eV. As described in Figure 5.b;c, the core level elemental peaks of UMA BPV and rGOZA were P 1p (133.9; 134 eV), C 1s (285.3; 285.4 eV), N 1s (400.1; 400.2 eV), O 1s (532.2; 532.3 eV), and Mg 1s (1304.4; 1304.6 eV) [17,57]. The mass fractions of P, C, N, O, and Mg found in rGOZA and UMA BPVs were evaluated to be 2.36; 2.24, 57.35; 58.3, 12.02;12.9, 25.71; 25.23, and 1.56;1.22% respectively. It's noteworthy to note that the mass fraction of C identified by XPS were 57.35 and 58.3% in rGOZA and UMA BPV struvite samples respectively, which were higher than any other elements, revealing more organics/biomass were concentrated on the surface of the

struvite sample. It is evident that organic molecules played a crucial role in the struvite morphogenesis through their surface binding [58]. The Mg 2p spectrum of rGOZA and UMA BPV (Fig. S1 a;b) was deconvoluted into the doublet peaks at 1304;1304.3 eV and 1305;1304.9 eV, which were likely corresponded to MgOH and MgO bonds, respectively [17,57]. Correspondingly, the P 2p spectrum of rGOZA and UMA BPV (Fig. S1 c;d) was divided into double peaks at approximately 133.3;133.4 eV and 134.2;134.3 eV, which matched to  $\text{PO}^-$  and POH, respectively [17,57].

The O 1s peak of rGOZA and UMA BPV (Fig. S1 e;f) was formed into three components at 531.5;531.3, and 533.3;533 eV, which matched to the MgOH, P = O, and POH bonds, respectively [17,57]. The atomic percentage ratios of Mg (At%): P (At%) for rGOZA and UMA BPV were 0.7 and 0.54, respectively, which were closely in concordance with the theoretical value of 1 [17,57], but it demands further optimization studies on the addition of Mg sources externally.

### **3.4 Electrochemical analyses**

#### **3.4.1 Polarization curve**

Both the rGO-zeolite modified and unmodified graphite felt-based human urine BPVs were operated in a batch cycle (5 days) with the supplement of neat human urine (undiluted). The BPVs were operated initially without connecting any external loads, the OCV was calculated for both the rGOZA and UMA-based human urine BPVs and exhibited a close range of values as  $962 \pm 8\text{mV}$  and  $895 \pm 7\text{mV}$ , respectively. But in the case of power density when BPVs operated against external resistance, the drop in the voltage range was reported with the remarkable difference among the variants of BPVs due to the variations in the anodic surface area particularly. All the BPVs were noticed with steady and stable performance with no remarkable variations in their electrochemical performance during the

time of fresh analyte replacement. The rGOZA and UMA-based human urine BPVs resulted in a stable operating voltage of  $271 \pm 0.5$  mV and  $185 \pm 0.4$  mV, respectively with the connected external resistor of  $100 \Omega$ . The polarization plot was obtained by disconnecting the external load and allowing the BPVs in the open circuit mode for 12 hours under the condition of zero current flow.

The polarization graphs were made for both the variants of BPVs by plotting current versus voltage, and current versus power (Fig. 6 a; b). The slope of the current versus voltage plot was utilized to estimate the developed internal resistance in BPV. The human urine BPVs with rGO and zeolite modified graphite felt anode exhibited lower internal resistance of  $159 \Omega$  than the BPVs with the unmodified anode as  $209.45 \Omega$ , due to the declined mass transfer diffusion and Ohmic losses. While most of the biological reactions take place on the anode's surface, the anode with a larger specific surface area gives microorganisms more room to bind over the anode (Fig. 4). In general, a large specific surface area represents two aspects: one is the apparent hierarchical structure, and the other is the porous structure [20]. The bacteria developing on the electrode scaffolds' surface primarily depends on the macropore structure to improve their contact with the electrodes; however, the micropores and mesopores can advance EET performance on the rGO surface [59]. Both the aspects can be fulfilled by using the rGO modified anode in the BES operation [20]. The synergistic effect of rGO and zeolites over the anode of rGOZA BPVs resulted in the peak power density of  $146.88 \text{ mW/m}^2$ , higher than the BPVs with the plain graphite felt anode of  $68.45 \text{ mW/m}^2$ . Most remarkably, the BPVs with rGO and zeolite modified anode reported the highest current density of  $1355 \text{ mA/m}^2$  which is greater than the previously reported study on acetate fed MFC with GO + zeolite anode ( $1070 \pm 7 \text{ mA/m}^2$ ) [32], and notably, urine fed MFC with the costlier CMI 7000 separators ( $461 \pm 0.1 \text{ mA/m}^2$ ) [60] respectively (Table.1). The rGOZA

BPVs have shown maximum power density than the other variant BPVs, which might be due to the property of the rGO that advanced lesser resistance during the charge transfer [61].

The BPVs were inoculated with the SUPER-MIX inocula as the biocatalyst than the pure strains [43]. Such a mutualistic approach of using heterogeneous microbial inoculum would have resulted in a higher power density and coulombic efficiency (CE) in BES [62]. It can be noted that the ohmic loss instigated by the internal electrochemical resistances amongst the tailor-made rGO- Zeolite anode and the biofilm were reduced, due to the fact of well-attached growth of the heterogeneous microbial biomass over the anode with a higher surface area [43]. The hindrance of the BPVs performance due to concentration losses was very less due to rapid oxidation of the organics in the human urine and the transportation of the generated electricity by the well-developed heterogeneous microbial biofilm over the rGO-zeolite modified anodes [4].

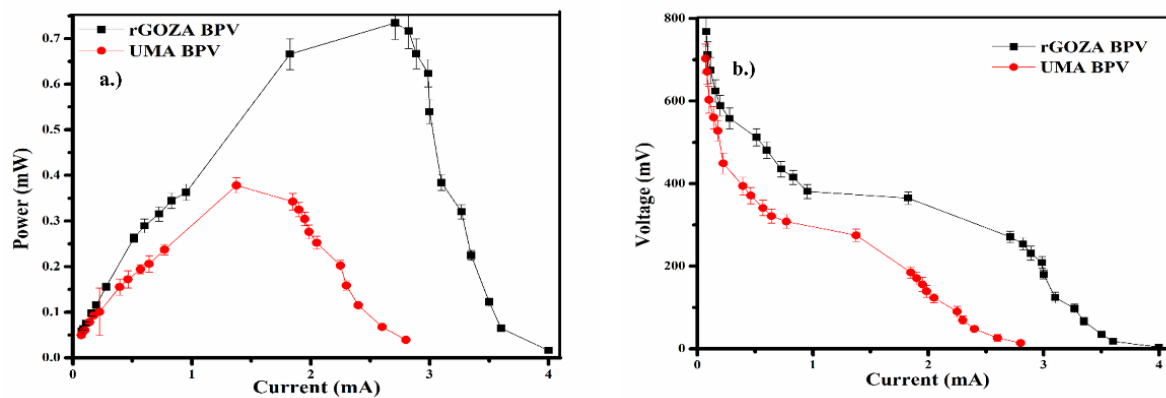


**Fig. 6** a.) Power curves of UMA and RGOZA BPV; b.) Polarization curves of UMA and RGOZA BPV

The human urine-powered BPV with the rGO-zeolite modified anode exhibited a peak power density of  $146.88 \text{ mW/m}^2$  and a current density of  $1355 \text{ mA/m}^2$  with the external load of  $100 \Omega$ . This achieved peak power density was 146.4 % higher than the BPV with the unmodified/bare graphite felt anode. Further, rGOZA BPVs resulted in lower internal resistance of  $159 \Omega$  along with improved biocatalytic activities by heterogeneous microbial

inocula at the peak current density region. But, due to microbial metabolic losses, the UMA BPVs signifies the higher concentration losses and inadequate microbial activities at low resistance, where the overshoot of power leads to low power output, as similarly reported earlier by Paul et al., 2018 [25]. Through the previous study, it is to be noted that there was no negative impact on microbial activities by adding the nanocomposite during the anode modification [63].

From the polarization curves (Fig. 6. a; b) of the variants of anode-based human urine BPVs, it is evident that rGO-zeolite modified anode-based BPVs with a higher surface area for the well-development of biofilm with the heterogeneous microbes would have aided to overcome the activation loss with improved power and current generation efficacy than the unmodified anode-based BPVs. The results of this analysis are expected to spark interest in future research in hybrid anodes for high-performance BPVs, and other bio-electrochemical systems.

1 **Table 1 Electrical and Overall Efficiency Comparison with Previous Studies**

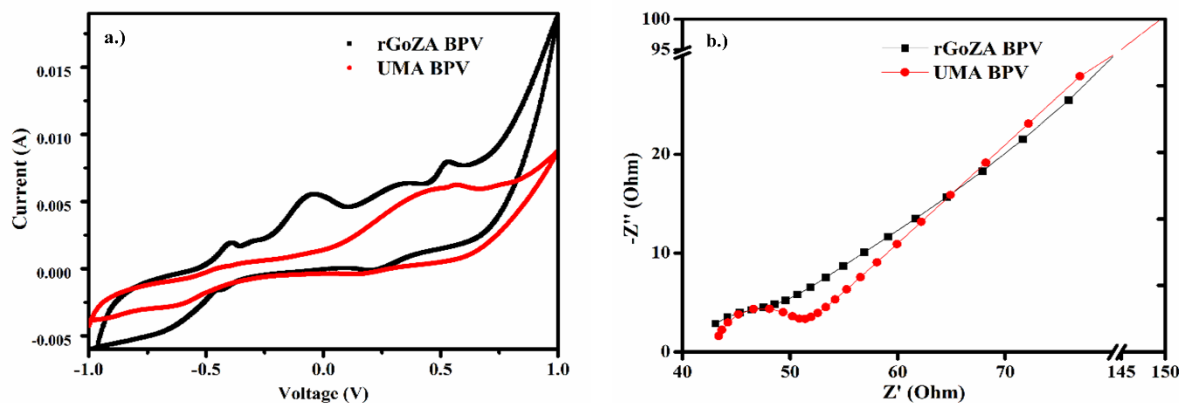
<b>Type of Anode</b>	<b>PEM</b>	<b>Substrate</b>	<b>Type of BES</b>	<b>Current Density (mA/m<sup>2</sup>)</b>	<b>COD Removal (%)</b>	<b>Coulombic Efficiency (%)</b>	<b>Reference</b>
rGOZA	Torch SeFparator	Human urine	BPV- Air cathode	1355	64 ± 4.96	15.16 ± 0.3	Current work
UMA	Torch Separator	Human urine	BPV- Air cathode	925	57 ± 4.2	11.6 ± 0.4	Current work
GO	Nafion	Acetate	MFC- Dual chamber	1000	83.7	37.6	[64]
GO+ Zeolite	Nafion	Acetate	MFC- Dual chamber	1070	85.9	44.1	[64]
S.S Mesh	Ultrex	Human urine	MFC- Dual chamber	450±4.27	75 ± 2.4	-	[60]

2

### 3.4.2 Cyclic voltammetry

CV is the most commonly utilized characterization technique to understand the bio-catalytic activities of the anodic microbial communities in the aspects of the current generation. It can also help to evaluate the generated current from the variants of the BPVs during the light/dark cycles with the applied variable potential [65]. Under the turnover condition the resulting redox peak current values can be used to correlate with the magnitude of the current generated through the bio-electrochemical activity (Fig. 7.a). The rGOZABPV with the rGO+Zeolite modified anode reported a higher catalytic redox current of 18.99 mA which is 2.15 times higher than UMA BPV with the unmodified anode.

The maximum redox catalytic peak currents of rGOZA BPVs depict the soluble redox shuttles generation by the anoxygenic phototropic bacteria with their synergistic participation in the effective electron transferring to the anodic surface [66]. Through the CV technique, the maximum redox catalytic peak current was revealed by the rGOZA BPVs during the steady-state and stable performance. Since rGO + zeolite has a larger surface area, the microbial biofilm and cell membrane-bound organelles can easily transfer free electrons to the anodic surface. This resulted in boosting electrochemical redox reactions through efficient electron transfer [46].



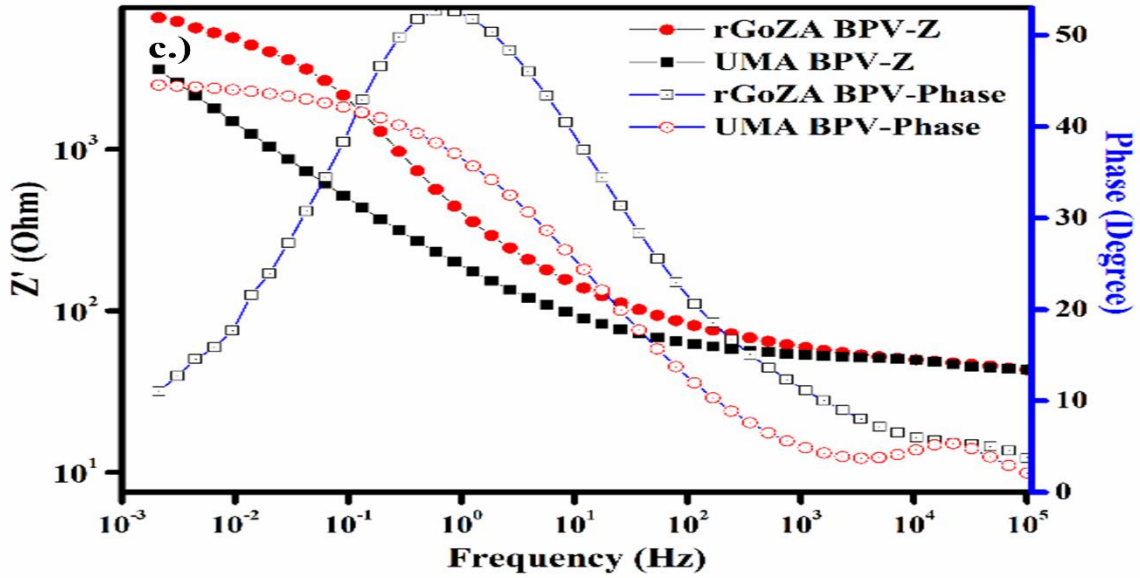


**Fig. 7** a.) Cyclic voltammograms for rGOZA BPV and UMA BPV; b.) Nyquist Plots for rGOZA BPV and UMA BPV during EIS analysis; and c.) Bode Plots for rGOZA BPV, and UMA BPV during EIS analysis;

### 3.4.3 Electrochemical impedance spectroscopy

The Nyquist plot revealed that EIS can be used to evaluate the developed internal resistance of the variants of clay separators based BPVs. The Nyquist plot provides the details about the prevailing solution or ohmic resistance ( $R_s$ ), polarization resistance ( $R_p$ ), and Warburg diffusion resistance ( $R_w$ ) at the anodic region qualitatively (Fig. 7.b). The solution resistance ( $R_s$ ) can be the difference between the origin point to the semicircle portion of the Nyquist plot, the polarization resistance ( $R_p$ ) can be the diameter of the semicircle and finally, the Warburg diffusion resistance ( $R_w$ ) can be the extending linear portion [50]. The BPV with the rGO + Zeolite modified anode has yielded the lowest ohmic resistance of  $42.8 \Omega$ , notable charge transfer resistance ( $6.25 \Omega$ ) along with the lesser Warburg diffusion limitations than the other variants of the torch separators powered urine BPVs. The qualitative  $R_s$ ,  $R_p$ , and  $R_w$  values of all the two variants of BPVs with rGOZA are

42.8  $\Omega$ ; 6.25  $\Omega$ ; 2  $\Omega$ , and UMA are 93.1  $\Omega$ ; 27.5  $\Omega$ ; 2  $\Omega$  through Nyquist plot respectively (Fig. 7. b).

The EIS results evidence the importance of employing a modified anode (rGOZA) with a higher surface area and pores for the fabrication of the torch-type clay separator-based urine BPVs for the optimal performance of the BPVs concerning both the aspects of power production, resource recovery, and higher pollutant removal efficiency. The mediator's response to a low amplitude AC signal over mid-frequency ranges was successfully analyzed using the Bode plot (Fig. 7.c). As shown in the figure, a drastic shift in peaks of phase angles as in the case of rGoZA-BPV represents the change in electrolyte conditions as well as improvement in oxidation reactions as compared to UMA-BPV. The rGOZA BPV revealed a better Constant Phase Element (CPE) of 648 nMho than UMA BPV of 244 nMho. The reduction in  $R_s$ , as seen in the Nyquist and Bode plot, is most likely due to greater proton movement to the cathode, similar to that noticed for increasing anodic catalytic conditions. Coating of rGO + zeolite on an anodic surface decreased the charge transfer impedance during the urine treatment and enhanced the kinetics of the electron transfer mechanism from the substrate to the anode, as similarly depicted from the polarization curve.

### **3.5 Outcome of pollutant removal and resource recovery**

In BES, the microbes digest and breakdown the organics fed in the anolyte for their cell maintenance and growth, followed by the liberation of free electrons and protons as bioelectricity [49]. The selection of microbial inocula and the anodic material with higher surface area to enhance the development of the biofilm during the operation of BPVs rely on the competence in the removal of COD and higher power production from the wastewater [43]. The rGO-zeolite modified graphite felt anode-based BPV attained maximum percentage removal efficiency of the organics and nutrients such as  $\text{NO}_3$ ,  $\text{NH}_4^+\text{-N}$ , and Ortho-P as  $47 \pm 0.3 \%$ ,  $49 \pm 0.5 \%$ , and  $88 \pm 0.3 \%$  respectively during the 5 days of batch mode cycle with

the neat urine as the anolyte. On the other hand, the BPVs with the unmodified graphite felt as anode reported a lower percentage removal efficiency of  $\text{NO}_3$ ,  $\text{NH}_4^+\text{-N}$ , and Ortho-P at  $38 \pm 0.21\%$ ,  $43 \pm 0.4 \%$ , and  $76 \pm 0.4 \%$  respectively (Table .2). Effective utilization of nutrients and organic carbon in electrochemical reactions resulted in higher pollutant removal efficiency in modified BPV over control BPV [46].

The maximal recovery of the resource in the form of clear catholyte was obtained from the rGO-zeolite modified graphite felt anode-based human urine BPVs of 8 ml/day which is 2.3 times higher than unmodified anode based BPVs with the externally connected resistor of  $100 \Omega$ . In MFCs, increasing current/power generation improves the flow of protons and other cations between electrodes, allowing more liquid to move from the anode to the cathode chamber [37]. The top functioning MFCs will result in a higher quantity of catholyte collection, and the linear relationship between power/current output and accumulated catholyte emphasizes the importance of electro-osmotic drag force [38].

The horizontal tube selection in the present study proposes the uniform mixing pattern for effective fluid dynamics and the suitability of such BPVs in pipe flow MFC during a decentralized wastewater collection system. The developed microbial biofilm over the anode utilized the available nutrients for their metabolism and growth. Due to this, the anolyte exhibits the complete and maximal reduction of Ortho-P and other nutrients respectively in the urine-fed BES [60,67]. The maximal COD removal efficiency attained during the human urine BPVs long-term operation was  $64 \pm 4.9\%$  with rGO-zeolite modified graphite felt anode and followed by  $57 \pm 4.2\%$  by unmodified graphite felt anode based BPVs. The rGO and its composite electrodes have been shown to improve the electricity generation efficiency of BES in numerous tests. The graphene-modified electrode's micron-sized pores not only avoided blocking caused by microbial attachment but also increased the EET performance and biocompatibility [68,69]. The performance of human urine BPVs with respect to COD

removal, and coulombic efficiency (CE) displays the adaptability, and scope of the BPVs for the effective human urine treatment, and onsite sanitation applications [43,70].

The attained values of maximal COD removal efficacy can be used to evaluate the CE of the human urine BPVs which relates the transformation of the provided chemical energy in the form of organic contaminants in the human urine into electrical power during the anaerobic digestion by the biocatalytic action of the microbes. The rGO-zeolite modified graphite felt anode-based human urine BPVs attained the maximum CE of  $15.16 \pm 0.3\%$  whereas the unmodified graphite felt anode-based BPVs reported with  $11.6 \pm 0.4\%$  based on the efficiency of the BPVs in COD removal (Table .2).

**Table. 2 Pollutant removal efficiency of Human urine BPVs**

<b>S.no</b>	<b>Parameters</b>	<b>Neat Urine</b>	<b>Treatment by Modified Anode Urine BPV</b>	<b>Treatment by Unmodified Anode urine BPV</b>
<b>1</b>	pH	$6.4 \pm 4$	$6.3 \pm 3$	$6.2 \pm 2$
<b>2</b>	Conductivity (mS/cm)	$12.1 \pm 0.5$	$5.2 \pm 0.6$	$6.3 \pm 0.4$
<b>3</b>	COD (g/L)	$11.5 \pm 0.2$	$4.14 \pm 0.1$ ( $64 \pm 4.96\%$ )	$4.95 \pm 0.2$ ( $57 \pm 4.2\%$ )
<b>4</b>	Ortho P (mg/L)	$185 \pm 12$	$22.2 \pm 3$ (88%)	$44.4 \pm 3.6$ (76%)
<b>5</b>	NH <sub>4</sub> N (mg/L)	$641 \pm 18$	$326.9 \pm 6$ (49%)	$365.37 \pm 7.3$ (43%)
<b>6</b>	NO <sub>3</sub> (mg/L)	$264 \pm 35$	$139.92 \pm 18$ (47%)	$163.68 \pm 15$ (38%)
<b>7</b>	C.E		$15.16 \pm 0.3$	$11.62 \pm 0.4$

The mixed or heterogeneous microbial cultures are mostly ideal than the pure cultures due to biofilm formation over the anodic surface [60]. With the well-developed heterogeneous microbial biofilm, the rGO-zeolite modified graphite felt anode promotes the consumption of additional organic pollutants for their growth, metabolism, and the preparedness of essential metabolic intermediates during the electron transport mechanism [43,71]. Thus, the combination of rGO with a higher specific surface area and a super-hydrophilic agent named zeolite over the anodic surface facilitated improved microbial colonization, subsequent enhanced anodic kinetics in the rGOZA based urine BPVs, which would have aided in the higher power density, COD removal, CE and recovery of struvite at ease.

### **3.6 Long term reliability and direct powering of Hygro-clock**

The long-term stability of BPVs is an important aspect to be assessed when using them in real-world applications. In this work, after the inoculation point, the BPVs were operated over a relatively long term of more than 6 months with an external resistance of  $100\Omega$  constantly. The BPVs were allowed to operate individually and favored the matured biofilm formation over the anode by supplying fresh urine as a substrate during the regular batch cycle's interval. Due to this, the BPVs were matured (after 8 days), the voltage generation, and pollutant removal performance remained stable for more than 180 days with stable electrochemical performance. During the steady-state performance phase (from 20-180 days) through the polarization study, the maximum yield of power generation from both the variants of BPVs was evaluated. The rGOZA powered horizontal torch-type urine fed BPVs reported a higher volumetric power density of  $146.882 \text{ mW/m}^2$  which is 2.16 times greater than the UMA BPVs. Overall, the rGOZA-based horizontal torch-type urine fed BPVs exhibited good long-term stability along with an outstanding performance with respect to power generation, COD removal, and struvite recovery than the UMA-based horizontal

torch-type urine fed BPVs (Table.2). Originally, the Hygro-clock required one AAA battery (1.5 V; 540mAh), even though there were triplicates of BPVs, only two individual horizontal torch-type urine fed BPVs from rGOZA/UMA variants were connected in series, resulting in a greater output voltage and more efficient use of electrical energy by reducing conversion losses [72].

The output OCV of two rGOZA and UMA horizontal torch-type urine fed BPVs series were 1.784 V and 1.51 V respectively. The BPVs were directly connected to the Hygro-clock after being exposed to open-circuit conditions for 1 hour (Fig. 1). There was no fluctuations/ malfunction in the Hygro-clock during the fixed 5 days of batch operation, most interestingly one-time filling of the rGOZA and UMA horizontal torch-type urine fed BPVs with neat human urine powered the Hygro-clock for 18 and 15 days respectively. Thus, simultaneous energy-resource recovery can be achieved in low-cost clay BPVs during human urine treatment and it was capable to operate the electronic appliances for onsite use.

### **3.7 Outlook and future perspectives**

As BPV is a technology with low current/power output, the limitation and reduction of cost are vital, hence the selection of the ion exchange separator and the modified electrode with a larger surface area is imposed. In general, improvements in electrode material characteristics and the use of low-cost separators would increase performance output while lowering the system's total cost [73]. In the present case, as anode electrode material, their suitability was tested for the first time in combination with the novel horizontally positioned clay torch type separator for enhanced urine treatment, electricity generation, struvite recovery, and clear catholyte collection. In particular, a clear catholyte collection as a resource is simple and easy as it does not involve the additional pump/suction units [39,40], which is an advantage in comparison to earlier studies on vertically positioned ceramic

separators with urine fed MFC [41,42]. It is evident through several previous reports that the reduced graphene oxide got good electrical conductivity, ensured a larger surface area for the microbial biofilm to adhere [74], and enhance electron transport to the electrode's surface by acting as a mediator [75]. Likewise, zeolite is known as molecular sieves which can increment the hydrophilicity of the anode with its porous structure helping the microbial anchorage [32].

On the surface of the novel torch ceramic separator that was exposed to air, there was less accumulation of salt deposits. The cathode portion of the novel horizontal torch type separator was exposed to the air, resulting in adequate hydration near the cathode area, allowing for easy recovery of the struvite-rich catholyte through electro-osmotic drag phenomena [38]. It is also to be noted that during the long-term operation of 180 days, there was no stagnation and also clear near the inner cathodic region exposed towards the separator due to the catholyte's antimicrobial properties [76]. This might be the reason for the BPV system's extended life, as it prevents cathode clogging, biofouling, and scaling. In the case of rGOZA-based horizontal torch type urine fed BPVs configuration in addition to enhancement in the power output, the rate of COD removal, and struvite recovery also improved. The appropriateness of the rGOZA combination with the horizontal torch-type clay separator for usage as an efficient BPV reactor is supported by both strong long-term stabilities and the system's resilience to changes in operating conditions, enhancing the technology's real-world deployment [77].

The feasibility and preliminary study on the essentials and suitability of rGOZA in horizontal torch-type urine fed BPV was attempted to generate power, COD removal, and struvite (slow-release fertilizer) recovery at ease without using any additional pump /suction gadgets from neat human urine. As a result, the current work pushes the boundaries even further by demonstrating that the system is a cost-effective, robust, and relatively compact

power source for laboratory Hygro-clocks. It is evident that better catholyte formation in rGOZA based BPV is strongly linked to current-induced ionic transport [78,79], which can result in ammonia recovery and stripping [9]. Recovery of valuable resources from urine would aid in the transition from energy-intensive treatments to resource production, as well as provide new technological prospects [38]. In urine, struvite crystals may get precipitated naturally, but the rate of reaction and purity can be enhanced by the addition of magnesium sources like artificial seawater,  $MgCl_2$ , and sea salts [37]. But apart from the potential benefits of the proposed system concept, special attention must be given to other design factors such as the addition of magnesium chloride for struvite precipitation [37], optimization of separator pore size for higher struvite recovery [38], and continuous mode of BPV operation [80]. Further, a detailed cost-benefit analysis is recommended for consideration, which can lead to sustainable energy in the future [81].

#### **4. Conclusions**

In the present study, rGO-zeolite modified anode (rGOZA) based BPVs with horizontal-torch type separator attained a higher power/current over bare anode with improved anode kinetics. The modified anode electrode promotes the electrocatalytic activities of redox reactions and hence improved the performance of BPVs for energy and resource recovery. For urine treatment, higher performance in ceramic-based BPVs promotes low-cost alternatives to the MFCs with the costlier Nafion and CMI separator. This proves the potential and possibility of using rGO-zeolite modified anode in human urine-fed BPVs for sanitation and scalable applications. Additionally, enhanced urine treatment, electricity generation, struvite recovery, and particularly, the collection of clear catholyte at ease without the use of any additional pump/suction gadgets under light at lower operating cost can be achieved by promoting a way forwards for sustainable development.

## **Acknowledgment**

Mr K. Gunaseelan is grateful to Pondicherry University for providing the UGC fellowship for the research work.

## **Conflict of Interest**

The authors declare that they have no known competing financial interests or personal relationships that could have appeared to influence the work reported in this paper.

## **Funding**

This research did not receive any specific grant from funding agencies in the public, commercial, or not-for-profit sectors.

## **Author CRediT contribution**

**KG:** Conceptualization, Methodology, Investigation, Formal analysis, Writing – original draft; **DAJ:** Data curation, Writing an original draft, Writing - review & editing; **DP:** Validation, Writing an original draft, Writing - review & editing; **SG:** Conceptualization, Validation, Resources, Writing - review & editing, Supervision.

## **Appendix A. Supplementary material**

E-supplementary data for this work can be found in the e-version of this paper online

## **References**

- [1] Bennetto HP, Stirling JL, Tanaka K, Vega CA. Anodic reactions in microbial fuel cells. *Biotechnol Bioeng* 1983;25:559–68. <https://doi.org/10.1002/bit.260250219>.
- [2] Bennetto HP. Electricity generation by microorganisms. *Biotechnology education*, 1(4), 163-168. 1990:163-168.
- [3] Suzuki, S., Karube, I. MT. *Application of a Biochemical Fuel Cell to Wastewaters*, Vol. 8, Tokyo Institute of Technology, Yokohama, 1997.

- [4] Chandra R, Venkata Subhash G, Venkata Mohan S. Mixotrophic operation of photo-bioelectrocatalytic fuel cell under anoxygenic microenvironment enhances the light dependent bioelectrogenic activity. *Bioresour Technol* 2012;109:46–56.  
<https://doi.org/10.1016/j.biortech.2011.12.135>.
- [5] Rosenbaum M, He Z, Angenent LT. Light energy to bioelectricity: Photosynthetic microbial fuel cells. *Curr Opin Biotechnol* 2010;21:259–64.  
<https://doi.org/10.1016/j.copbio.2010.03.010>.
- [6] Vélez-Pérez LS, Ramirez-Nava J, Hernández-Flores G, Talavera-Mendoza O, Escamilla-Alvarado C, Poggi-Varaldo HM, et al. Industrial acid mine drainage and municipal wastewater co-treatment by dual-chamber microbial fuel cells. *Int J Hydrogen Energy* 2020;45:13757–66. <https://doi.org/10.1016/j.ijhydene.2019.12.037>.
- [7] Rewatkar P, Enaganti PK, Rishi M, Mukhopadhyay S, Goel S. Single-step inkjet-printed paper-origami arrayed air-breathing microfluidic microbial fuel cell and its validation. *Int J Hydrogen Energy* 2021;46:35408–19.  
<https://doi.org/10.1016/j.ijhydene.2021.08.102>.
- [8] Ieropoulos I, Greenman J, Melhuish C. Urine utilisation by microbial fuel cells; energy fuel for the future. *Phys Chem Chem Phys* 2012;14:94–8.  
<https://doi.org/10.1039/C1CP23213D>.
- [9] Kuntke P, Śmiech KM, Bruning H, Zeeman G, Saakes M, Sleutels THJA, et al. Ammonium recovery and energy production from urine by a microbial fuel cell. *Water Res* 2012;46:2627–36. <https://doi.org/https://doi.org/10.1016/j.watres.2012.02.025>.
- [10] Ieropoulos IA, Greenman J, Melhuish C. Miniature microbial fuel cells and stacks for urine utilisation. *Int J Hydrogen Energy* 2013;38:492–6.  
<https://doi.org/10.1016/j.ijhydene.2012.09.062>.

- [11] Xiao Y, Li Y, Ning Z, Li P, Yang P, Liu C, et al. Organic contaminant removal efficiency of sodium bentonite/clay (BC) mixtures in high permeability regions utilizing reclaimed wastewater: A meso-scale study. *J Contam Hydrol* 2018;210:1–14. <https://doi.org/10.1016/j.jconhyd.2018.01.008>.
- [12] Yadav G, Mishra A, Ghosh P, Sindhu R, Vinayak V, Pugazhendhi A. Technical, economic and environmental feasibility of resource recovery technologies from wastewater. *Sci Total Environ* 2021;796:149022. <https://doi.org/https://doi.org/10.1016/j.scitotenv.2021.149022>.
- [13] Santoro C, Babanova S, Artyushkova K, Atanassov P, Greenman J, Cristiani P, et al. The effects of wastewater types on power generation and phosphorus removal of microbial fuel cells (MFCs) with activated carbon (AC) cathodes. *Int J Hydrogen Energy* 2014;39:21796–802. <https://doi.org/https://doi.org/10.1016/j.ijhydene.2014.09.167>.
- [14] Merino Jimenez I, Brinson P, Greenman J, Ieropoulos I. Electronic faucet powered by low cost ceramic microbial fuel cells treating urine. *J Power Sources* 2021;506:230004. <https://doi.org/https://doi.org/10.1016/j.jpowsour.2021.230004>.
- [15] Santoro C, Ieropoulos I, Greenman J, Cristiani P, Vadas T, Mackay A, et al. Power generation and contaminant removal in single chamber microbial fuel cells (SCMFCs) treating human urine. *Int J Hydrogen Energy* 2013;38:11543–51. <https://doi.org/10.1016/j.ijhydene.2013.02.070>.
- [16] Tremouli A, Greenman J, Ieropoulos I. Effect of simple interventions on the performance of a miniature MFC fed with fresh urine. *Int J Hydrogen Energy* 2021;46:33594–600. <https://doi.org/10.1016/j.ijhydene.2021.07.171>.
- [17] Liao M, Liu Y, Tian E, Ma W, Liu H. Phosphorous removal and high-purity struvite

- recovery from hydrolyzed urine with spontaneous electricity production in Mg-air fuel cell. *Chem Eng J* 2020;391:123517.  
<https://doi.org/https://doi.org/10.1016/j.cej.2019.123517>.
- [18] Salar-García MJ, Ieropoulos I. Optimisation of the internal structure of ceramic membranes for electricity production in urine-fed microbial fuel cells. *J Power Sources* 2020;451:227741. <https://doi.org/10.1016/j.jpowsour.2020.227741>.
- [19] Walter XA, Santoro C, Greenman J, Ieropoulos I. Self-stratifying microbial fuel cell: The importance of the cathode electrode immersion height. *Int J Hydrogen Energy* 2019;44:4524–32. <https://doi.org/https://doi.org/10.1016/j.ijhydene.2018.07.033>.
- [20] Yu F, Wang C, Ma J. Applications of graphene-modified electrodes in microbial fuel cells. *Materials (Basel)* 2016;9. <https://doi.org/10.3390/ma9100807>.
- [21] Lai M-F, Lou C-W, Lin J-H. 3D composite electrodes of microbial fuel cells used in livestock wastewater: Evaluations of coating and performance. *Int J Hydrogen Energy* 2017;42:27666–76. <https://doi.org/https://doi.org/10.1016/j.ijhydene.2017.07.021>.
- [22] Papaharalabos G, Greenman J, Melhuish C, Ieropoulos I. A novel small scale Microbial Fuel Cell design for increased electricity generation and waste water treatment. *Int J Hydrogen Energy* 2015;40:4263–8.  
<https://doi.org/https://doi.org/10.1016/j.ijhydene.2015.01.117>.
- [23] Geetanjali, Rani R, Sharma D, Kumar S. Optimization of operating conditions of miniaturize single chambered microbial fuel cell using NiWO<sub>4</sub>/graphene oxide modified anode for performance improvement and microbial communities dynamics. *Bioresour Technol* 2019;285:121337. <https://doi.org/10.1016/j.biortech.2019.121337>.
- [24] Lin XQ, Li ZL, Liang B, Nan J, Wang AJ. Identification of biofilm formation and

- exoelectrogenic population structure and function with graphene/polyaniline modified anode in microbial fuel cell. *Chemosphere* 2019;219:358–64.  
<https://doi.org/10.1016/j.chemosphere.2018.11.212>.
- [25] Zhou S, Lin M, Zhuang Z, Liu P, Chen Z. Biosynthetic graphene enhanced extracellular electron transfer for high performance anode in microbial fuel cell. *Chemosphere* 2019;232:396–402. <https://doi.org/10.1016/j.chemosphere.2019.05.191>.
- [26] Mashkour M, Rahimnejad M, Pourali SM, Ezoji H, ElMekawy A, Pant D. Catalytic performance of nano-hybrid graphene and titanium dioxide modified cathodes fabricated with facile and green technique in microbial fuel cell. *Prog Nat Sci Mater Int* 2017;27:647–51. <https://doi.org/10.1016/j.pnsc.2017.11.003>.
- [27] Liu J, Qiao Y, Guo CX, Lim S, Song H, Li CM. Graphene/carbon cloth anode for high-performance mediatorless microbial fuel cells. *Bioresour Technol* 2012;114:275–80. <https://doi.org/10.1016/j.biortech.2012.02.116>.
- [28] González T, Ureta-Zañartu MS, Marco JF, Vidal G. Effect of Zeolite-Fe on graphite anode in electroactive biofilm development for application in microbial fuel cells. *Appl Surf Sci* 2019;467–468:851–9. <https://doi.org/10.1016/j.apsusc.2018.10.120>.
- [29] Qiao Y, Wu XS, Ma CX, He H, Li CM. A hierarchical porous graphene/nickel anode that simultaneously boosts the bio- and electro-catalysis for high-performance microbial fuel cells. *RSC Adv* 2014;4:21788–93. <https://doi.org/10.1039/c4ra03082f>.
- [30] Walcarius A. Zeolite-modified electrodes in electroanalytical chemistry. *Anal Chim Acta* 1999;384:1–16. [https://doi.org/10.1016/S0003-2670\(98\)00849-6](https://doi.org/10.1016/S0003-2670(98)00849-6).
- [31] Valdés MG, Pérez-Cordoves AI, Díaz-García ME. Zeolites and zeolite-based materials in analytical chemistry. *TrAC - Trends Anal Chem* 2006;25:24–30.

- <https://doi.org/10.1016/j.trac.2005.04.016>.
- [32] Paul D, Noori MT, Rajesh PP, Ghangrekar MM, Mitra A. Modification of carbon felt anode with graphene oxide-zeolite composite for enhancing the performance of microbial fuel cell. *Sustain Energy Technol Assessments* 2018;26:77–82.  
<https://doi.org/10.1016/j.seta.2017.10.001>.
- [33] Man mohan K, V KK, Harindran S V., Gajalakshmi S. Biosorptionally treated dye wastewater employed in “Olla-pot coupled microbial fuel cell” for tomato (*Solanum lycopersicum* L.) irrigation and bio-electricity production. *Bioresour Technol Reports* 2021;13:100626. <https://doi.org/10.1016/j.biteb.2021.100626>.
- [34] V KK, Man K, Manangath SP, Manju P, Gajalakshmi S. Resource recovery from paddy field using plant microbial fuel cell. *Process Biochem* 2020;99:270–81.  
<https://doi.org/10.1016/j.procbio.2020.09.015>.
- [35] Yousefi V, Mohebbi-Kalhari D, Samimi A. Ceramic-based microbial fuel cells (MFCs): A review. *Int J Hydrogen Energy* 2017;42:1672–90.  
<https://doi.org/10.1016/j.ijhydene.2016.06.054>.
- [36] Zinadini S, Zinatizadeh AA, Rahimi M, Vatanpour V, Bahrami K. Energy recovery and hygienic water production from wastewater using an innovative integrated microbial fuel cell–membrane separation process. *Energy* 2017;141:1350–62.  
<https://doi.org/https://doi.org/10.1016/j.energy.2017.11.057>.
- [37] Merino-Jimenez I, Celorrio V, Fermin DJ, Greenman J, Ieropoulos I. Enhanced MFC power production and struvite recovery by the addition of sea salts to urine. *Water Res* 2017;109:46–53. <https://doi.org/https://doi.org/10.1016/j.watres.2016.11.017>.
- [38] Gajda I, Greenman J, Santoro C, Serov A, Atanassov P, Melhuish C, et al. Multi-

- functional microbial fuel cells for power, treatment and electro-osmotic purification of urine. *J Chem Technol Biotechnol* 2019;94:2098–106.  
<https://doi.org/10.1002/jctb.5792>.
- [39] Cid CA, Stinchcombe A, Ieropoulos I, Hoffmann MR. Urine microbial fuel cells in a semi-controlled environment for onsite urine pre-treatment and electricity production. *J Power Sources* 2018;400:441–8. <https://doi.org/10.1016/j.jpowsour.2018.08.051>.
- [40] Merino Jimenez I, Brinson P, Greenman J, Ieropoulos I. Electronic faucet powered by low cost ceramic microbial fuel cells treating urine. *J Power Sources* 2021;506:230004. <https://doi.org/10.1016/j.jpowsour.2021.230004>.
- [41] Gajda I, Greenman J, Ieropoulos I. Microbial Fuel Cell stack performance enhancement through carbon veil anode modification with activated carbon powder. *Appl Energy* 2020;262:114475.  
<https://doi.org/https://doi.org/10.1016/j.apenergy.2019.114475>.
- [42] Merino-Jimenez I, Gonzalez-Juarez F, Greenman J, Ieropoulos I. Effect of the ceramic membrane properties on the microbial fuel cell power output and catholyte generation. *J Power Sources* 2019;429:30–7. <https://doi.org/10.1016/j.jpowsour.2019.04.043>.
- [43] Gunaseelan K, Jadhav DA, Gajalakshmi S, Pant D. Blending of microbial inocula: An effective strategy for performance enhancement of clayware Biophotovoltaics microbial fuel cells. *Bioresour Technol* 2021;323.  
<https://doi.org/10.1016/j.biortech.2020.124564>.
- [44] Cheng S, Liu H, Logan BE. Increased performance of single-chamber microbial fuel cells using an improved cathode structure. *Electrochem Commun* 2006;8:489–94.  
<https://doi.org/10.1016/j.elecom.2006.01.010>.

- [45] Gautam RK, Bhattacharjee H, Venkata Mohan S, Verma A. Nitrogen doped graphene supported  $\alpha$ -MnO<sub>2</sub> nanorods for efficient ORR in a microbial fuel cell. *RSC Adv* 2016;6:110091–101. <https://doi.org/10.1039/C6RA23392A>.
- [46] Jadhav DA, Ghangrekar MM. Effective ammonium removal by anaerobic oxidation in microbial fuel cells. *Environ Technol (United Kingdom)* 2015;36:767–75. <https://doi.org/10.1080/09593330.2014.960481>.
- [47] Beatty JT, Overmann J, Lince MT, Manske AK, Lang AS, Blankenship RE, et al. An obligately photosynthetic bacterial anaerobe from a deep-sea hydrothermal vent. *Proc Natl Acad Sci U S A* 2005;102:9306–10. <https://doi.org/10.1073/pnas.0503674102>.
- [48] Ihekwebe GO, Shondo JN, Orisekeh KI, Kalu-Uka GM, Nwuzor IC, Onwualu AP. Characterization of certain Nigerian clay minerals for water purification and other industrial applications. *Heliyon* 2020;6:e03783. <https://doi.org/https://doi.org/10.1016/j.heliyon.2020.e03783>.
- [49] Logan BE, Regan JM. Microbial Fuel Cells—Challenges and Applications. *Environ Sci Technol* 2006;40:5172–80. <https://doi.org/10.1021/es0627592>.
- [50] Ghadge AN, Ghangrekar MM. Development of low cost ceramic separator using mineral cation exchanger to enhance performance of microbial fuel cells. *Electrochim Acta* 2015;166:320–8. <https://doi.org/10.1016/j.electacta.2015.03.105>.
- [51] (1995) A. American Public Health Association (1995) Standard Methods for the Examination of Water and Wastewater, 19th edition. APHA, Washington, DC, USA n.d.
- [52] Shin YE, Sa YJ, Park S, Lee J, Shin KH, Joo SH, et al. An ice-templated, pH-tunable self-assembly route to hierarchically porous graphene nanoscroll networks. *Nanoscale*

- 2014;6:9734–41. <https://doi.org/10.1039/c4nr01988a>.
- [53] Wu X yuan, Tong F, Song T shun, Gao X ying, Xie J jing, Zhou CC, et al. Effect of zeolite-coated anode on the performance of microbial fuel cells. *J Chem Technol Biotechnol* 2015;90:87–92. <https://doi.org/10.1002/jctb.4290>.
- [54] Goto Y, Yoshida N, Umeyama Y, Yamada T, Tero R, Hiraishi A. Enhancement of electricity production by graphene oxide in soil microbial fuel cells and plant microbial fuel cells. *Front Bioeng Biotechnol* 2015;3:1–8. <https://doi.org/10.3389/fbioe.2015.00042>.
- [55] Suguna K, Thenmozhi M, Sekar C. Growth, spectral, structural and mechanical properties of struvite crystal grown in presence of sodium fluoride. *Bull Mater Sci* 2012;35:701–6. <https://doi.org/10.1007/s12034-012-0322-6>.
- [56] You J, Greenman J, Melhuish C, Ieropoulos I. Electricity generation and struvite recovery from human urine using microbial fuel cells. *J Chem Technol Biotechnol* 2016;91:647–54. <https://doi.org/10.1002/jctb.4617>.
- [57] Wei L, Hong T, Li X, Li M, Zhang Q, Chen T. New insights into the adsorption behavior and mechanism of alginic acid onto struvite crystals. *Chem Eng J* 2019;358:1074–82. <https://doi.org/https://doi.org/10.1016/j.cej.2018.10.110>.
- [58] Li H, Yao QZ, Yu SH, Huang YR, Chen XD, Fu SQ, et al. Bacterially mediated morphogenesis of struvite and its implication for phosphorus recovery. *Am Mineral* 2017;102:381–90. <https://doi.org/10.2138/am-2017-5687>.
- [59] He Z, Liu J, Qiao Y, Li CM, Thatt T, Tan Y. *Nano Lett.* 2012;12:4738–4. <https://doi.org/10.1021/nl202222a011>.
- [60] Sharma P, Mutnuri S. Nutrient recovery and microbial diversity in human urine fed

- microbial fuel cell. *Water Sci Technol* 2019;79:718–30.  
<https://doi.org/10.2166/wst.2019.089>.
- [61] Wang G, Qian F, Saltikov CW, Jiao Y, Li Y. Microbial Reduction of Graphene Oxide by *Shewanella* 2011;4. <https://doi.org/10.1007/s12274-011-0112-2>.
- [62] D.A. Jadhav and M.M. Ghangrekar. Optimising the proportion of pure and mixed culture in inoculum to enhance the performance of microbial fuel cells. *Int J Environ Technol Manag* 2020.
- [63] Mehdinia A, Ziaei E, Jabbari A. Facile microwave-assisted synthesized reduced graphene oxide/tin oxide nanocomposite and using as anode material of microbial fuel cell to improve power generation. *Int J Hydrogen Energy* 2014;39:10724–30.  
<https://doi.org/10.1016/j.ijhydene.2014.05.008>.
- [64] Paul D, Noori MT, Rajesh PP, Ghangrekar MM, Mitra A. Modification of carbon felt anode with graphene oxide-zeolite composite for enhancing the performance of microbial fuel cell. *Sustain Energy Technol Assessments* 2018;26:77–82.  
<https://doi.org/10.1016/j.seta.2017.10.001>.
- [65] Cereda A, Hitchcock A, Symes MD, Cronin L, Bibby TS, Jones AK. A bioelectrochemical approach to characterize extracellular electron transfer by *synechocystis* sp. PCC6803. *PLoS One* 2014;9:1–8.  
<https://doi.org/10.1371/journal.pone.0091484>.
- [66] Raghavulu SV, Modestra JA, Amulya K, Reddy CN, Venkata Mohan S. Relative effect of bioaugmentation with electrochemically active and non-active bacteria on bioelectrogenesis in microbial fuel cell. *Bioresour Technol* 2013;146:696–703.  
<https://doi.org/10.1016/j.biortech.2013.07.097>.

- [67] Jadhav DA, Deshpande PA, Ghangrekar MM. Enhancing the performance of single-chambered microbial fuel cell using manganese/palladium and zirconium/palladium composite cathode catalysts. *Bioresour Technol* 2017;238:568–74. <https://doi.org/10.1016/j.biortech.2017.04.085>.
- [68] Yong YC, Yu YY, Yang Y, Li CM, Jiang R, Wang X, et al. Increasing intracellular releasable electrons dramatically enhances bioelectricity output in microbial fuel cells. *Electrochem Commun* 2012;19:13–6. <https://doi.org/10.1016/j.elecom.2012.03.002>.
- [69] Tang J, Chen S, Yuan Y, Cai X, Zhou S. In situ formation of graphene layers on graphite surfaces for efficient anodes of microbial fuel cells. *Biosens Bioelectron* 2015;71:387–95. <https://doi.org/10.1016/j.bios.2015.04.074>.
- [70] Jadhav DA, Das I, Ghangrekar MM, Pant D. Moving towards practical applications of microbial fuel cells for sanitation and resource recovery. *J Water Process Eng* 2020;38:101566. <https://doi.org/10.1016/j.jwpe.2020.101566>.
- [71] Jadhav DA, Jain SC, Ghangrekar MM. Cow's urine as a yellow gold for bioelectricity generation in low cost clayware microbial fuel cell. *Energy* 2016;113:76–84. <https://doi.org/10.1016/j.energy.2016.07.025>.
- [72] Walter XA, Santoro C, Greenman J, Ieropoulos IA. Scalability and stacking of self-stratifying microbial fuel cells treating urine. *Bioelectrochemistry* 2020;133. <https://doi.org/10.1016/j.bioelechem.2020.107491>.
- [73] Sharma R, Kumari R, Pant D, Malaviya P. Bioelectricity generation from human urine and simultaneous nutrient recovery: Role of Microbial Fuel Cells. *Chemosphere* 2022;292:133437. <https://doi.org/https://doi.org/10.1016/j.chemosphere.2021.133437>.
- [74] Chen M, Zeng Y, Zhao Y, Yu M, Cheng F, Lu X, et al. Monolithic three-dimensional

- graphene frameworks derived from inexpensive graphite paper as advanced anodes for microbial fuel cells. *J Mater Chem A* 2016;4:6342–9.  
<https://doi.org/10.1039/c6ta00992a>.
- [75] Liu J, Qiao Y, Guo CX, Lim S, Song H, Li CM. Graphene/carbon cloth anode for high-performance mediatorless microbial fuel cells. *Bioresour Technol* 2012;114:275–80. <https://doi.org/10.1016/j.biortech.2012.02.116>.
- [76] Gajda I, Greenman J, Melhuish C, Ieropoulos IA. Electricity and disinfectant production from wastewater: Microbial Fuel Cell as a self-powered electrolyser. *Sci Rep* 2016;6:1–9. <https://doi.org/10.1038/srep25571>.
- [77] Jadhav DA, Mungray AK, Arkatkar A, Kumar SS. Recent advancement in scaling-up applications of microbial fuel cells: From reality to practicability. *Sustain Energy Technol Assessments* 2021;45:101226.  
<https://doi.org/https://doi.org/10.1016/j.seta.2021.101226>.
- [78] Kim JR, Premier GC, Hawkes FR, Dinsdale RM, Guwy AJ. Development of a tubular microbial fuel cell (MFC) employing a membrane electrode assembly cathode. *J Power Sources* 2009;187:393–9.  
<https://doi.org/https://doi.org/10.1016/j.jpowsour.2008.11.020>.
- [79] Rozendal RA, Hamelers HVM, Buisman CJN. Effects of membrane cation transport on pH and microbial fuel cell performance. *Environ Sci Technol* 2006;40:5206–11.  
<https://doi.org/10.1021/es060387r>.
- [80] Sabin JM, Leverenz H, Bischel HN. Microbial fuel cell treatment energy-offset for fertilizer production from human urine. *Chemosphere* 2022;294:133594.  
<https://doi.org/https://doi.org/10.1016/j.chemosphere.2022.133594>.

- [81] Jadhav DA, Park S-G, Pandit S, Yang E, Ali Abdelkareem M, Jang J-K, et al.  
Scalability of microbial electrochemical technologies: Applications and challenges.  
Bioresour Technol 2022;345:126498.  
<https://doi.org/https://doi.org/10.1016/j.biortech.2021.126498>.